Precisely Shaped Acoustic Ablation of Tumors Utilizing Steerable Needle and 3D Ultrasound Image Guidance

Emad M. Boctor[1], Philipp Stolka[1], Hyun-Jae Kang[1], Clyde Clarke[1], Caleb Rucker[2], Jordan Croom[2], E. Clif Burdette[3] , Robert J. Webster III[2]

[1] Department of Radiology, Johns Hopkins University, Baltimore, MD USA
[2] Department of Mechanical Engineering, Vanderbilt University, Nashville, TN USA
[3] Acoustic MedSystems, Inc., Champaign, IL USA

ABSTRACT

Many recent studies have demonstrated the efficacy of interstitial ablative approaches for the treatment of hepatic tumors. Despite these promising results, current systems remain highly dependent on operator skill, and cannot treat many tumors because there is little control of the size and shape of the zone of necrosis, and no control over ablator trajectory within tissue once insertion has taken place. Additionally, tissue deformation and target motion make it extremely difficult to place the ablator device precisely into the target. Irregularly shaped target volumes typically require multiple insertions and several overlapping (thermal) lesions, which are even more challenging to accomplish in a precise, predictable, and timely manner without causing excessive damage to surrounding normal tissues.

In answer to these problems, we have developed a steerable acoustic ablator called the ACUSITT with the ability of directional energy delivery to precisely shape the applied thermal dose. In this paper, we address image guidance for this device, proposing an innovative method for accurate tracking and tool registration with spatially-registered intraoperative three-dimensional US volumes, without relying on an external tracking device. This method is applied to guidance of the flexible, snake-like, lightweight, and inexpensive ACUSITT to facilitate precise placement of its ablator tip within the liver, with ablation monitoring via strain imaging. Recent advancements in interstitial high-power ultrasound applicators enable controllable and penetrating heating patterns which can be dynamically altered. This paper summarizes the design and development of the first synergistic system that integrates a novel steerable interstitial acoustic ablation device with a novel trackerless 3DUS guidance strategy.

Keywords: Ultrasound, Steerable Needle, Robot, Liver, Image-Guided Surgery, Ablation, Elasticity Imaging, Sensorless 3DUS

1. INTRODUCTION

Hepatocellular carcinoma (HCC) is the most common type of common primary liver cancer with over one million new cases worldwide per year. In the United States HCC incidence is increasing, largely due to known and clinically occult hepatitis C [El-Serag-2003]. Other primary malignancies are also on the rise in the U.S., including intrahepatic cholangiocarcinoma [DeOliveira-2007]. However, metastatic diseases from other sites are the most common hepatic malignancies in the U.S. overall. Colorectal cancer accounts for the majority of these metastases, although other primary gastrointestinal, lung, and breast tumors (among others) also commonly cause hepatic metastases. For colorectal cancer specifically, 146,000 new cases were diagnosed in 2005 and 50% of these (73,000 patients) developed liver metastases with 30% (44,000 patients) exhibiting metastases confined exclusively to the liver [McLoughlin-2006].

In selected patients, potentially curative therapies for primary and secondary liver cancer include surgical resection and in some cases liver transplantation. Unfortunately only a small percentage of patients are candidates for these treatments. Intra-arterial approaches such as chemoembolization, while therapeutically useful in some cases, rarely achieve complete tumor destruction. For these reasons, interest has increased in interstitial ablative approaches for the treatment of primary and metastatic liver cancer, including chemical ablation, cryoablation [Kuszyk-2000], and radiation therapy [Koniaris-2000]. Perhaps most promising is the use of heat ablation using energy sources like radiofrequency (RF) [Cho-

*eboctor@jhmi.edu; phone 1 443 287 2975; http://musiic.lcsr.jhu.edu

ti-2000, Choti-2002a], laser, microwave [Izumi-2001], or focused ultrasound [Daum-1999, Haar-1995]. These thermal approaches utilize image guided placement of a probe within the target area in the liver parenchyma. High frequency interstitial focused ultrasound has been developed partially in response to the limitations of other ablative approaches such as cryotherapy and RFA.

In spite of promising results of ablative therapies, significant technical barriers exist with regard to its efficacy, safety, and applicability to many patients. Specifically, these limitations include: (1) control of current ablative therapy technology, (2) localization/targeting of the tumor, and (3) monitoring of the ablation zone.

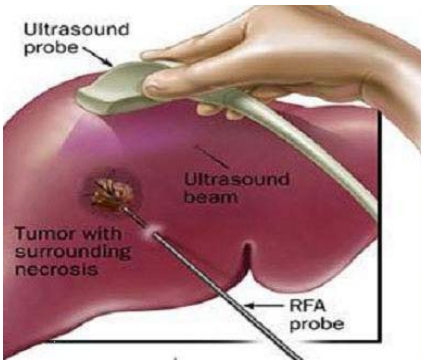

Figure 1. Radiofrequency ablation of a liver tumor under 2D US.

Current Ablation Technology Limitation: Many recent studies have demonstrated the efficacy of interstitial ablative approaches for the treatment of hepatic tumors, including chemical ablation, cryoablation, and thermal ablation using energy sources like radiofrequency, laser, microwave, or focused ultrasound. Despite these promising results, current systems remain highly dependent on operator skill, and cannot treat many tumors because there is insufficient control of the size and shape of the zone of necrosis, and no control over the ablator trajectory within the tissue.

Targeting Limitation: One common feature of current ablative methodologies is the necessity for precise placement of the end-effector tip in specific locations, typically within the volumetric center of the tumor, in order to achieve adequate destruction. The tumor and a zone of surrounding normal parenchyma can then be ablated. Tumors are identified by preoperative imaging, primarily CT and MR, and then localized by intra-operative ultrasonography (IOUS) (Figure 1). When performed percutaneously, trans-abdominal ultrasonography is most commonly used. One major limitation of ablative approaches is the lack of accuracy in probe localization within the center of the tumor. In addition, manual guidance often requires multiple passes and repositioning of the ablator tip, further increasing the risk of bleeding and tumor dissemination. In situations when the desired target zone is larger than a single ablation size (e.g. 5-cm tumor and 4-cm ablation device), multiple overlapping spheres are required in order to achieve complete tumor destruction. In such cases, the capacity to accurately execute multiple manual ablations is significantly impaired by the geometrically complex 3D planning required as well as by image distortion artifacts from the first ablation, further reducing the targeting confidence and potential efficacy of the therapy. IOUS often provides excellent visualization of tumors and guidance for probe placement, but its 2D nature and dependence on the sonographer's skills limit its effectiveness [Wood-2000].

Monitoring Limitation: Current monitoring approaches often result in either local failure or in excessively large zones of liver ablation. Some ablative devices employ temperature monitoring using thermistors built into the ablation probes. However, these temperature readings only provide a crude estimate of the zone of ablation. Non-invasive monitoring techniques include ultrasound imaging, magnetic resonance imaging, computed tomography, X-ray fluoroscopy, and elasticity imaging. The main advantage of an ultrasound-based monitoring approach is that it can be utilized and applied intraoperatively during the intervention without moving the patient to the MRI or CT scanner room or exploiting X-ray radiation.

Our Approach: Improved real-time guidance for planning, delivery, and monitoring of the ablative therapy would provide the missing capability needed to enable accurate and effective application of this promising therapy. Recent studies are beginning to identify reasons for diminished efficacy of ablative approaches, including size, location, operator experience, and technical approach [van Duijnhoven-2006]. These studies suggest that device targeting and ablation monitoring are likely the key reasons for local failure.

However, real-time ablation monitoring will be particularly useful if coupled to an ablative technology capable of precisely shaping the delivered thermal dose in real-time. Recent studies have demonstrated significant advantages of multi-transducer interstitial ultrasound applicators, most notably the capability to dynamically tailor the longitudinal and angular heating distributions which are important for conformable treatments and preserving critical non-targeted tissue [Diederich-1999, Nau-1999, Nau-2007]. Therefore, a strong rationale exists for studying interstitial therapeutic ultrasound as a modality for thermal therapy, together with real-time monitoring imaging feedback.

In this paper, we introduce the first synergistic prototype that integrates the following three technologies: 1) Ultrasonic Interstitial Thermal Therapy (USITT) device [Diederich-1999, 1999a], 2) Steerable Active Cannula (AC) [Web-

ster-2006] that delivers the ablation tool, and 3) Trackerless 3DUS and real-time ultrasound elasticity imaging for guidance and monitoring of the deposited thermal energy. In this project, we started to develop an innovative method for accurate tracking and tool registration with respect to spatially-registered intraoperative US volumes without relying on an external tracking device. This three-dimensional ultrasound (3DUS) will be integrated with a flexible, snake-like lightweight and inexpensive robotic, called the Active Cannula (AC), to facilitate precise placement of a steerable ultrasound thermal ablator into the liver and to monitor the progress of tissue ablation with real-time 3D registered ultrasound. Recent developments of implantable or interstitial high-power ultrasound applicators have demonstrated extremely controllable and penetrating heating patterns which can be shaped and dynamically altered, providing an ideal mechanism for conformable thermal surgery.

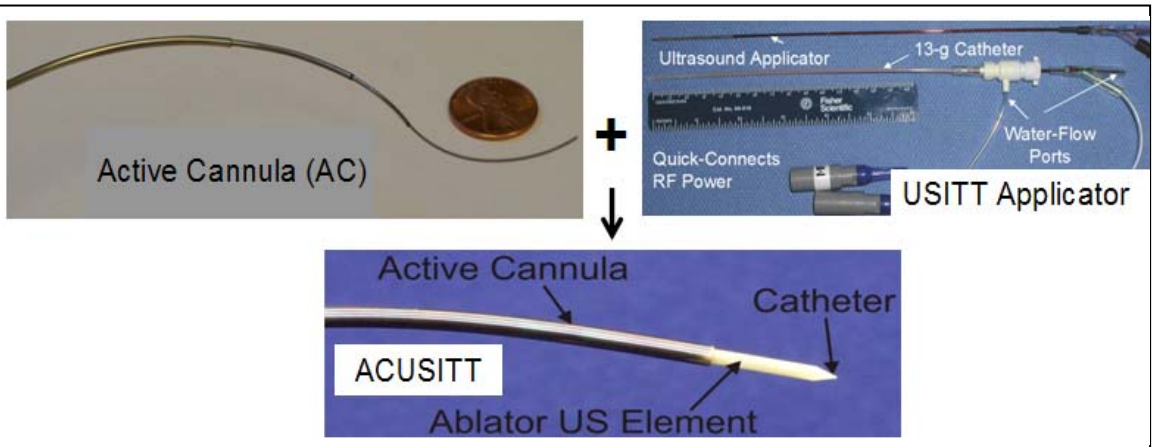

Figure 2. Active Cannula with Ultrasonic Interstitial Thermal Therapy (ACUSITT) applicator. Top-Left: A prototype 4-tube active cannula (AC). Top-Right: Ultrasound Interstitial Thermal Therapy (USITT) flexible interstitial ultrasound applicators designed for heating from within catheters. Bottom: Photo of an ACUSITT tip showing the USITT ablator delivered through an AC.

2. METHODS

2.1 The Active Cannula with Ultrasonic Interstitial Thermal Therapy (ACUSITT) Device

The USITT interstitial ultrasound applicators utilize arrays of small tubular ultrasound radiators [Diederich-1996, Diederich-1999] (Figure 2, Top-Right). The applicators contain multiple tubular segments, each with separate power control, so that the energy deposition can be adjusted in real time along the applicator axis. Each transducer delivers highly collimated energy, so that the axial shape of the therapeutic temperature zone is well defined by the number of active elements and their applied power levels. Angular control of energy delivery is also possible by sectoring the transducer surface at e.g. 90°, 180°, or 360°. The Active Cannula (AC) is built from several concentric precurved elastic tubes (Figure 2, Top-Left). When these tubes are actuated to axially extend and rotate, the shape and trajectory of the AC change accordingly. Integrating the AC and USITT is conceptually simple. Since the USITT is flexible, it can be delivered through the central working channel of an AC with appropriately sized tubes. The experimental prototype used in our studies is shown in Figure 2.

2.2 Trackerless 3DUS System

We developed an integrated prototype for an image-based sensorless 3DUS system [Rivaz-2006, -2007a] implemented in C++. The prototype system consists of both hardware and software components. The hardware side comprises a Sonix RP system (Ultrasonix Medical Corporation) for acquisition of ultrasound (*US*) data and a robotic stage for μm-precise

positioning of the US probe to provide ground-truth displacement information; the software components integrate and command the hardware as well as perform the offline and online computations.

The system operates in two distinct modes – *calibration mode* and *image-based 3DUS reconstruction mode*. Both are described in the following from a process flow perspective (Figure 3). In calibration mode, information necessary to calibrate the later distance estimations is collected. To this end, the robot control component steps the robot through a series of precisely defined positions and triggers the acquisition of a single US frame (RF data) from a homogeneous fully developed speckle (*FDS*) phantom at each position. These frames are associated with their respective coordinates and stored for offline use. Then, the software system reads the batch of frames and positions and subdivides the frames into distinct subpatches. Pairs of patches at the same location originating from frames at different distances are then correlated, thus creating a set of (strictly monotonous) calibration (or decorrelation) curves $\Gamma_{x,y}(d)$. These curves depend on the characteristics of the selected probe, the imaging frequency, and the image location x, y (in particular the depth y) of the respective patches. Currently, the offline calibration process takes 2-3 minutes including scan time to generate the needed decorrelation curves.

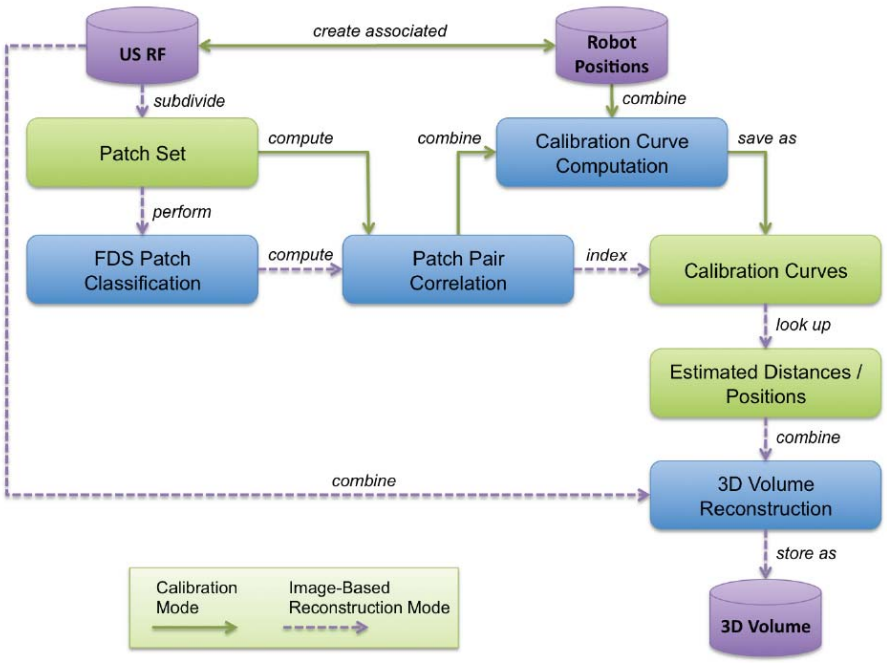

Figure 3. Trackerless 3DUS process flow.

In image-based 3DUS reconstruction mode, the distances $d_{i,j}$ between successive frames f_i, f_j are computed. We need at least three distance measurements to determine a unique plane (for the current frame) with respect to the neighboring or previously scanned planes. The same robot-based system is used to acquire US frames from a phantom, providing *ground truth* distances for performance evaluation. The robot is also capable of introducing translational in-plane and out-of-plane motions, which makes this setup an ideal testing platform. Again, a batch of frames is acquired and transferred *en bloc* to the distance estimation algorithm. For each patch, the same patch subdivision as before is performed, and FDS patches are selected in an FDS classification phase. This subset of patches is correlated with corresponding patches from a set of preceding frames (chosen as described below), resulting in decorrelation values $CC_{i,j}$ which serve as lookup indices into the previously computed decorrelation curves, yielding a set of distance estimates Δd (Figure 4). From this set, a single distance or position estimate $d_{i,j}$ is computed by averaging.

We investigated three different patch distance estimation algorithms. In the <u>*accumulation approach*</u>, patches from each new frame f_n are correlated to their counterparts from only the immediately preceding frame f_{n-1}. However, the decorrelation curves hint at certain correlations resulting in better estimates than others. To overcome this limitation, we investigated a method that gives high weight to more trusted correlation patch pairs. In the <u>*weighted average approach*</u>, patches from preceding frames $f_{n-1} \ldots f_{n-m}$ are used for correlation (m corresponding to the domain of the decorrelation

curve), with their resulting estimates being weighted according to the derivative $\Gamma_{x,y}'(d)$ of the corresponding decorrelation curve (Figure 4). Finally, the *maximum weight approach* selects only the distance/weight pair with the highest weight.

In both calibration and image-based reconstruction modes, the patch size can be reduced by the introduction of US *beam steering*. Two frames are acquired at the same position with different beam angles, resulting in (partly) independent speckle patterns. Then, the size of each patch can be cut by half, thereby increasing the probability of finding high-quality patches with minimal coherent scattering components [Rivaz-2007b]. The two half-sized patches from the same positions are reassembled into one structure, which then undergoes FDS classification.

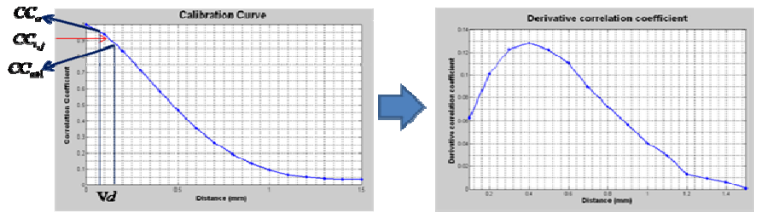

Figure 4. Decorrelation curve (for a particular patch depth) and its derivative.

2.3 Real-time GPU-based Elasticity Imaging System

We applied parallelization to the calculation of strain images using multi-core Nvidia general-purpose GPU cards [Boctor-2009]. These graphics processing units contain many cores, typically ranging from 128 to 240 or more. Each core can be dedicated to perform various functions on different sets of data. Nvidia has provided a parallel computing architecture named CUDA (Compute Unified Device Architecture), which is used for programming and configuring these GPU's. It defines a thread block, which – as its name suggests – is a group of threads. A piece of function called kernel can be configured to run on a particular number of blocks, and each thread in those blocks performs the same function as specified in the kernel on the same or a different dataset. In this multi-threaded programming, it is important that the functions (in our case the kernels) be thread safe, ensuring that they do not update global data or shared data without synchronization.

The GPU-based system component is integrated with the real-time RF acquisition, beam steering, and B-mode reconstruction components (Figure 5), following a modular, distributed architecture. With this functional breakdown of the solution into a collection of independent, communicating modules, we achieve efficient resource allocation across different machines, high module cohesion, as well as decoupling of modules to minimize the impact of processing performance discrepancies. In its current implementation and configuration, the modules span up a directed, acyclic communications graph as nodes, with communication channels like network and shared memory (depending on distribution vs. co-location and one-to-one vs. one-to-many configuration) as edges.

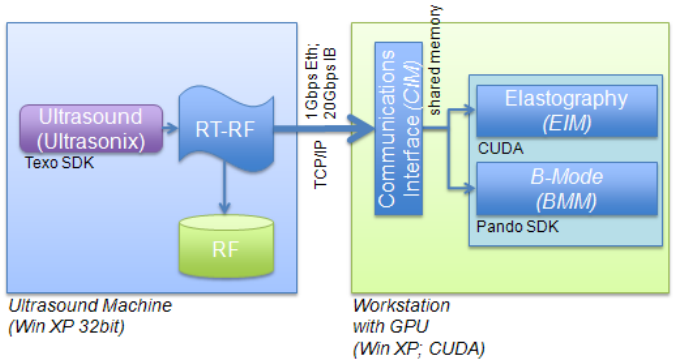

Figure 5. Part of the distributed software architecture. Real-time RF data is acquired through the communication interface module (CIM) and distributed to both B-mode and elasticity modules.

2.4 Experimental Testbed

Figure 6 shows the experimental testbed of the integration of the active cannula (AC) and the ultrasound ablator tool (USITT) under real-time ultrasound guidance. The shown setup is used for positioning the ACUSITT tip and the US imaging probe mounted on the µm-precise positioning robot. This robot is included to provide "ground truth" for the proposed trackerless 3DUS method. Scans were taken for three positions of the ACUSITT tip controlled by the mechanism of Figure 2 through a single tissue insertion point as depicted in Figure 6.

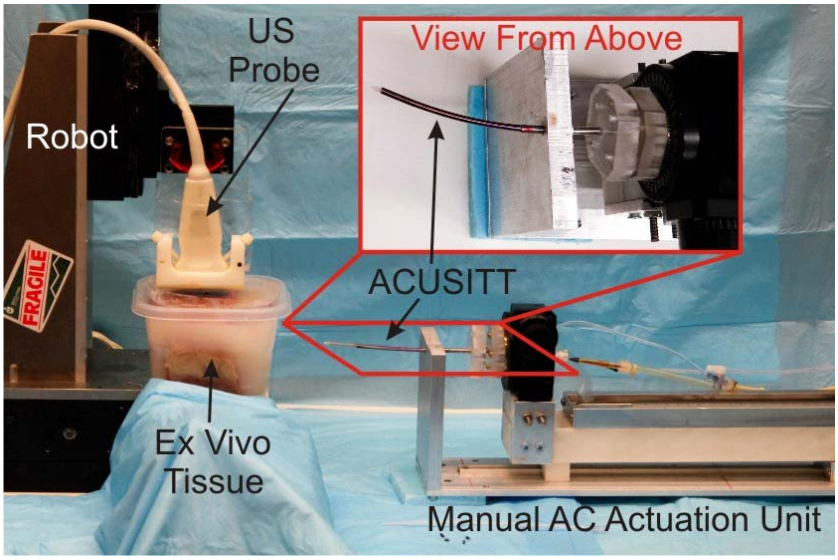

Figure 6. Setup used for 3DUS volume reconstruction and ACUSITT tip localization.

3. EXPERIMENTAL RESULTS

The ACUSITT device testing and integration is described and presented in a separate paper [Burdette-2010]. In this section, we will describe different experiments and results pertaining to the following: 1) image-based 3DUS component, 2) real-time elasticity imaging system, and 3) ex vivo tissue experiments that integrate for the first time the AC and USITT tools under ultrasound guidance.

3.1 Trackerless 3DUS System Results

The *accumulation approach* was used during ex-vivo tissue experiments to perform "trackerless" reconstruction of three positions deployed by the integrated ACUSITT device. The results were compared to ground truth robot position data. Figure 6 shows the setup used for positioning the ACUSITT tip and the US imaging probe mounted on the *µm*-precise positioning robot. Scans were taken for three positions of the ACUSITT tip controlled by the mechanism of Figure 2 through a single tissue insertion point as depicted in Figure 7. Figure 8 is the result of an experiment including three ACUSITT tip positions and shows the ground truth and 3DUS results. After introducing these three fiducials, a 3DUS scan was performed with 149 images and covering around 60 mm scanning distance (out-of-plane). While pa-

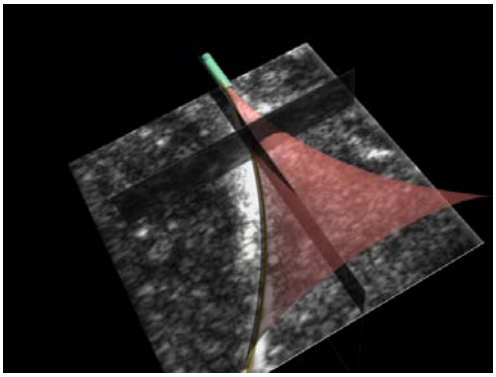

Figure 7. Representation of ACUSITT within the US volume, showing one pose within the workspace (red overlay).

rallel scanning and image-based reconstruction can preserve axial and lateral resolution, it is known that accurate recovery of the out-of-plane motion is always a challenging task with unavoidable drift. Figure 8 shows that out-of-plane motion can be recovered with only 11% drift error using the accumulation method. This method depends on our novel work in FDS classification and accurate resolution cell calibration [Rivaz-2006, 2007a]. Figure 9 compares the 3D reconstruction of the three fiducials from both ground truth and the sensorless 3DUS method.

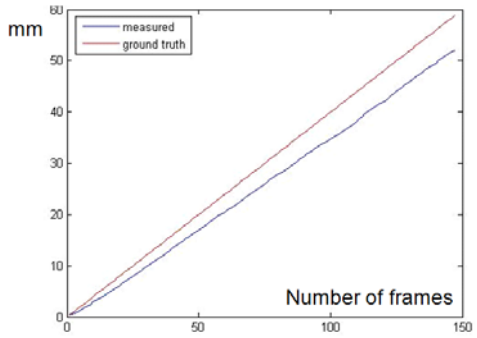

Figure 8. Results of 3DUS reconstruction versus ground truth for three ACUSITT positions in ex-vivo bovine muscle tissue performed for 149 scans over 60mm.

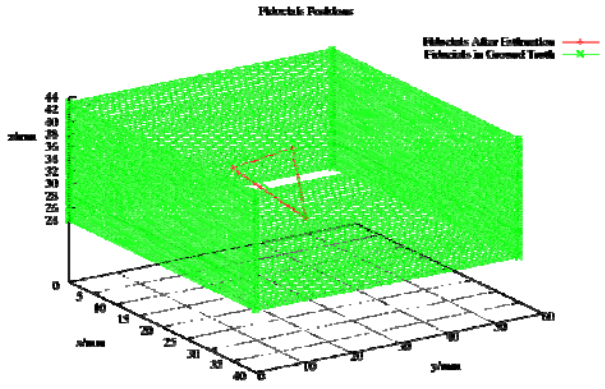

Figure 9. Comparison of 3D reconstruction of the inserted three fiducial markers using both ground-truth and the sensorless image-based method. As shown, the image-based method causes the three fiducials to deviate less than 1-2mm compared to ground truth. These deviations can be easily compensated by the ACUSITT. (The triangle vertices represent the locations of three cylindrical metal fiducial markers, while the green squares represent the individual ultrasound image planes.)

The time required to reconstruct a 3DUS volume using the proposed sensorless method is a function of the following three tasks: 1) scan time, 2) FDS patch classification, 3) distance estimation and 3DUS reconstruction. In general, scanning a volume of interest might take from 2 – 5 seconds depending on the size of the VOI and scan speed. During this time, the generated volume consists of 40 – 250 frames (with ultrasound frame rate ranges from 20 – 50 frames/sec, depending on the imaging settings). Typically, 100 – 150 images are the average size of a single 3DUS volumetric scan. Methods 2 and 3 (as shown in Figure 10) require on average less than 25 milliseconds, depending on the chosen algorithm and method. This time is calculated per pair of images, which means the algorithm run time for 100 images is approximately 2.5 seconds.

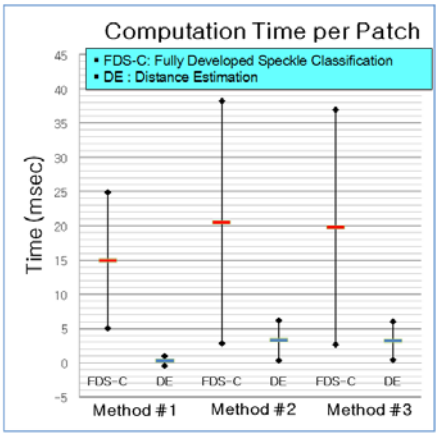

Figure 10. Image-based 3DUS reconstruction time. Method 1 is the accumulation approach; method 2 is the weighted average approach; and method 3 is the maximum weight approach.

3.2 Real-time Elasticity Imaging Results

The parallelized implementation of the normalized cross-correlation elasticity imaging method using CUDA has been tested on an NVidia GeForce 9800 GX2 GPU card with 512 MB RAM and with an Intel Quad Core Q9400 CPU host CPU and 8GB RAM. First we studied the performance of our code on the GPU card as a function of both the volume size and the number of sample points (strain points per RF line) [Boctor-2009]. The volume size ranges from 1 to 750 images per volume. Typically, this parameter is in the range of 50-200 images per volume. Another study has been performed where we have fixed the number of sampling points to 139. Equivalent C implementation performance is also shown in Figure 11. As expected, it is observed that the CUDA implementation is much faster than the C implementation. Specifically, the speedup is about 28x if we do not take into account the I/O time to transfer the data between the host (CPU) memory and the device (GPU) memory. With the I/O taken into consideration, it is still 22x faster.

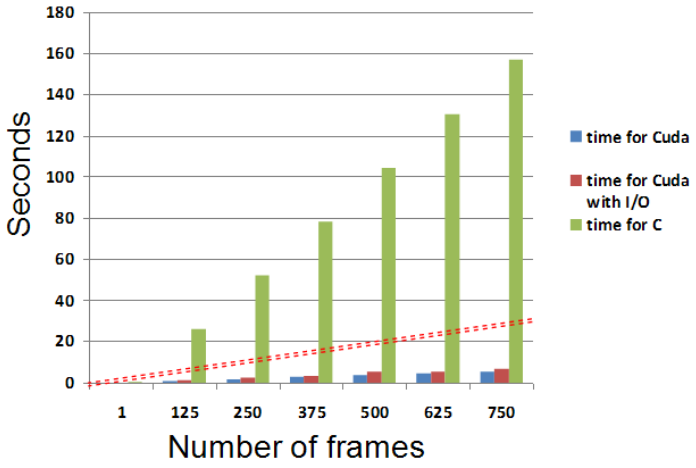

Figure 11. GPU performance time vs. *C* implementation. The dotted line shows the time needed to acquire these volumes using an ultrasound acquisition rate of 30 frames/sec, defining the real-time threshold. It is apparent that the GPU-based EI method is faster than this deadline.

3.3 Ultrasound-guided ACUSITT Prototype Results

Additionally, we integrated ultrasound imaging to guide and monitor ablation using the first ACUSITT prototype, as shown in Figure 6. This experiment demonstrates combined spatial planning and thermal modeling, which resulted in accurate targeting of the treatment zones. Furthermore, these results are confirmed with both elasticity images and gross-pathology pictures. Figure 12 shows strain images taken after performing three controlled ablations from a single entry point using the ACUSITT device. Strain results are in good correspondence with gross-pathology outcomes.

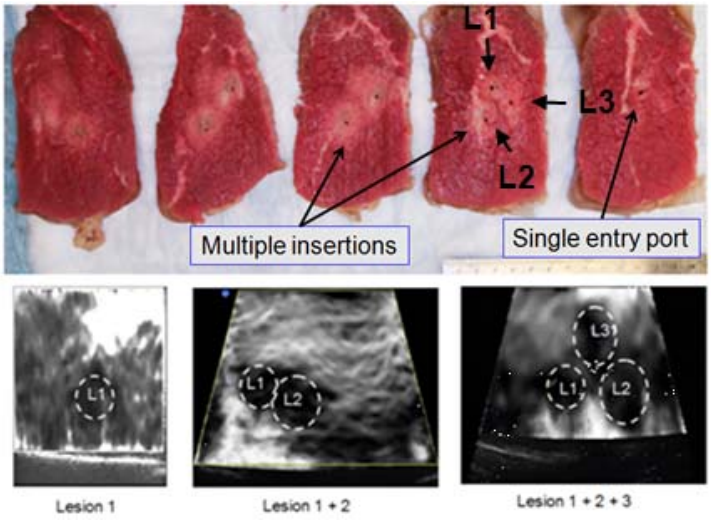

Figure 12. Intraoperative monitoring of ablative therapy using strain imaging. Gross-pathology pictures confirm strain images and highlight the ability of performing multiple insertions from a single entry port using the ACUSITT tool.

4. CONCLUSION

In this work, we presented the first integrated prototype comprising the following components: AC delivery system, USITT ablation tool, and trackerless real-time strain ultrasound imaging system. This new system is capable of applying multiple ablations from a single entry point, eliminating the need for multiple insertions using current and available ablation technologies. Moreover, targeting can be performed under the guidance of a low-cost image-based 3DUS system. While drift error is unavoidable with image-based 3DUS reconstruction, the design redundancy of both AC maneuverability and USITT changeable ablation pattern can overcome this limitation. Additionally, real-time elasticity imaging provides a valuable feedback to the ACUSITT tool, allowing to precisely shape the desired ablation. While this paper presents a first prototype, there is more to be added to the current system implementation including: extending the current sensorless 3DUS algorithms to include the beam steering aspect in real-time, integrating monitoring information with the ACUSITT device, and conducting animal in-vivo trials to test the overall navigation accuracy of the proposed novel system.

In summary, the results from the prototype presented in this paper demonstrates the potential to provide a low-cost, closed-loop system for steering, placement with a single parenchymal penetration, and guidance and percutaneous delivery of conformal ultrasound ablative therapy with on-line monitoring.

ACKNOWLEDGEMENTS

The authors would like to thank Drs. Gregory Hager, Russell Taylor, Iulian Iordachita, Michael Choti, Mr. Nishikant Deshmukh, and Mr. Hassan Rivaz. This work has been supported by NIH SBIR Grant CA134169, NSF EEC 9731478, Radiology Intramural Grant and a National Science Foundation Graduate Research Fellowship.

REFERENCES

[Boctor2008] E. M. Boctor, M. A. Choti, E. C. Burdette, and R. J. Webster III. Three-Dimensional Ultrasound-Guided Robotic Needle Placement: An Experimental Evaluation. International Journal of Medical Robotics and Computer Assisted Surgery, 4(2), 180-191, 2008.

[Boctor-2009] Boctor EM, Deshmukh N, Ayad M, Clarke C, Dickie K, Burdette E. Three-Dimensional Heat-induced Echo-Strain Imaging for Monitoring Interstitial High Intensity Ablation. The International Society for Optical Engineering (SPIE) on Medical Imaging 2009, Vol. 7265, 72650R.

[Burdette-2010] Burdette EC, Rucker DC, Prakash P, Diederich CJ, Croom JM, Clarke C, Stolka PJ, Juang T, Boctor EM, Webster III RJ, “The ACUSITT ultrasonic ablator: the first steerable needle with an integrated interventional tool” SPIE Medical Imaging 2010.

[Choti-2000] Choti MA, “Hepatic radiofrequency ablation,” The Cancer Journal 2000; 6(4): 291-2.

[Choti-2002a] Choti MA, “Surgical management of hepatocellular carcinoma: resection and ablation,” J Vasc Interv Radiol. 2002 Sep;13 (9 Suppl):S197-203.

[Daum-1999] D. R. Daum, N. Smith, N. McDannald, K. H. Hynynen, "MR guided noninvasive thermal coagulation of in vivo liver tissue using ultrasonic phased array," In: T. Ryan, T. R. Wong (eds) Thermal treatment of tissue with image guidance, proceedings of SPIE. pp. 185-195, 1999

[DeOliveira-2007] DeOliveira ML, Cunningham SC, Cameron JL, Kamangar F, Winter JM, Lillemoe KD, Choti MA, Yeo CJ, Schulick RD, “Cholangiocarcinoma: Thirty-one-Year Experience With 564 Patients at a Single Institution,” Ann Surg. 2007 May; 245(5): 755–762

[Diederich-1996] C. J. Diederich,"Ultrasound applicators with integrated catheter-cooling for interstitial hyperthermia: theory and preliminary experiments," Int. J. Hyperthermia, vol. 12, no. 2, pp. 279-297, 1996.

[Diederich-1999] C. J. Diederich, W. H. Nau, D. Deardorff, E.C. Burdette, P. R. Stauffer, "Ultrasound technology for thermal therapy: interstitial and intracavitary approaches," IEEE Trans. Biomed. Eng., 1999, no.2, pp. 1268-1277.

[Diederich-1999a] C. J. Diederich, W. H. Nau, P. R. Stauffer, "Ultrasound applicators for interstitial thermal coagulation," IEEE Trans. Ultrason., Ferroelect., Freq. Contr., vol.46, no.5 pp. 1218-1228.

[El-Serag-2003] El-Serag HB, Davila JA, Petersen NJ, McGlynn KA., "The continuing increase in the incidence of hepatocellular carcinoma in the United States: an update," Ann Intern Med. 2003 Nov 18;139(10):817-23.

[Haar-1995] G. ter Haar,"Ultrasound focal beam surgery," Ultrasound Med. Biol., vol. 21, no. 9, pp. 1089-100, 1995]

[Izumi-2001] Izumi N, Asahina Y, Noguchi O, Uchihara M, Kanazawa N, Itakura J, Himeno Y, Miyake S, Sakai T, Enomoto N, "Risk factors for distant recurrence of hepatocellular carcinoma in the liver after complete coagulation by microwave or radiofrequency ablation," Cancer. 2001 Mar 1;91 (5):949-56.

[Koniaris-2000] Koniaris LG, Chan DY, Magee C, Solomon SB, Anderson JH, Smith DO, DeWeese T, Kavoussi LR, Choti MA, "Focal hepatic ablation using interstitial photon radiation energy," J Am Coll Surg. 2000 Aug;191(2):164-74.

[Kuszyk-2000] Kuszyk BS, Boitnott JK, Choti MA, Bluemke DA, Sheth S, Magee CA, Horton KM, Eng J, Fishman EK, "Local tumor recurrence following hepatic cryoablation: radiologic-histopathologic correlation in a rabbit model," Radiology. 2000 Nov;217 (2):477-86.

[McLoughlin-2006] McLoughlin JM, Jensen EH, Malafa M, "Resection of Colorectal Liver Metastases: Current Perspectives," Cancer Control. 2006;13(1):32-41.

[Nau-1999] W. H. Nau, C. J. Diederich,"Directional power deposition from direct-coupled and catheter-cooled interstitial ultrasound applicators," Int. J. Hyperthermia, vol. (In Press), no. pp. 1999

[Nau-2007] W. H. Nau, C. J. Diederich, J Simko, T Juang, A Jacoby, E. C. Burdette, Ultrasound Interstitial Thermal Therapy for the Treatment of Uterine Myomas, SPIE Proceedings, San Jose, Jan. 2007

[Rivaz-2006] Rivaz H, Boctor EM, Fichtinger G. Ultrasound Speckle Detection Using Low Order Moments. IEEE Ultrasonics Symposium 2006, pp. 2092-2095.

[Rivaz-2007a] Rivaz H, Boctor EM, Fichtinger G. A Robust Meshing and Calibration Approach for Sensorless Freehand 3D Ultrasound. The International Society for Optical Engineering (SPIE) on Medical Imaging 2007, Vol. 6513, pp. 651318_1-8.

[Rivaz-2007b] Rivaz H, Zellars R, Hager G, Fichtinger G, Boctor EM. Beam Steering Approach to Speckle Characterization and Out-of-Plane Motion Estimation in Real Tissue. IEEE Ultrasonics Symposium 2007, pp. 781 – 784.

[van Duijnhoven – 2006] van Duijnhoven FH, Jansen MC, Junggeburt JM, van Hillegersberg R, Rijken AM, van Coevorden F, van der Sijp JR, van Gulik TM, Slooter GD, Klaase JM, Putter H, Tollenaar RA, "Factors influencing the local failure rate of radiofrequency ablation of colorectal liver metastases," Ann Surg Oncol. 2006 May;13(5):651-8. Epub 2006 Mar 17.

[Webster-2006] Webster III RJ, Kim, JS, Cowan NJ, Chirikjian GS, Okamura AM "Nonholonomic modeling of needle steering," International Journal of Robotics Research, 25(5/6):509–526, May/June 2006

[Wood-2000] Wood TF, Rose DM, Chung M, Allegra DP, Foshag LJ, Bilchik AJ, "Radiofrequency ablation of 231 unresectable hepatic tumors: indications, limitations, and complications," Ann Surg Oncol. 2000 Sep;7 (8):593-600